A Comprehensive Quasi-3D Model for Regional-Scale Unsaturated-Saturated Water Flow

Wei Mao[1], Yan Zhu[1]*, Heng Dai[2], Ming Ye[3], Jinzhong Yang[1], Jingwei Wu[1]

[1]State Key Laboratory of Water Resources and Hydropower Engineering Science, Wuhan University, Wuhan, Hubei 430072, China.

[2]Institute of Groundwater and Earth Sciences, Jinan University, Guangzhou, Guangdong 32306, China.

[3]Department of Earth, Ocean, and Atmospheric Science, Florida State University, Tallahassee, FL 32306, USA.

* Corresponding Author: Yan Zhu

Phone: 86-2768775432; Email: zyan0701@163.com; Fax: 86-2768776001

Abstract: For computationally efficient modeling of unsaturated-saturated flow in regional scales, the Quasi three-dimensional (3-D) scheme that considering one-dimensional (1-D) soil water flow and 3-D groundwater flow is an alternative method. However, it is still practically challenging for regional-scale problems due to the high non-linear and intensive input data needed for soil water modeling and the reliability of the coupling scheme. This study developed a new Quasi-3D model coupled the 1-D soil water balance model UBMOD with the 3-D hydrodynamic model MODFLOW. A new implementation method of the iterative scheme was developed, in which the vertical net recharge and unsaturated zone depth were used as the exchange information. A modeling framework was developed to organize the coupling scheme of the soil water model and the groundwater model and to handle the pre- and the post-processing information. The strength and weakness of the coupled model were evaluated by using two published studies. The comparison results show that the coupled model is satisfactory in terms of computational accuracy and mass balance error. The influence of spatial and temporal discretization as well as the stress period on the model accuracy were discussed. Additionally, the coupled model was used to evaluate groundwater recharge in a real-world study. The measured groundwater table and soil water content were used to calibrate the model parameters, and the groundwater recharge data from a two years' tracer experiment was used to evaluate the recharge estimation. The field application further shows the practicability of the model. The developed model and the modeling framework provide a convenient and flexible tool for evaluating unsaturated-saturated flow system at the regional scale.

1 Introduction

While groundwater resource is important for the domestic, agricultural, and industrial uses, groundwater is vulnerable due to over-exploitation, climate change, and

49 biochemical pollution (Bouwer, 2000; Sophocleous, 2005; Evans and Sadler, 2008;
50 Karandish et al., 2015; Zhang et al., 2018). For protecting or exploiting groundwater
51 resource, understanding soil water flow system is necessary as soil water is the major
52 source of groundwater recharge and destination of phreatic consumption (Yang et al.,
53 2016; Wang et al., 2017). The Richards' equation is usually used to describe the soil
54 water flow and groundwater flow. Many numerical schemes have been developed to
55 solve the three-dimensional (3-D) Richards' equation (Weill et al., 2009) in computer
56 codes, such as HYDRUS (Šimůnek et al., 2012), FEFLOW (Diersch, 2013),
57 HydroGeoSphere (Brunner and Simmons, 2012), InHM (VanderKwaak and Loague,
58 2001) and MODHMS (Tian et al., 2015). These fully 3-D models have solid theoretical
59 foundation, and have been used for regional scale unsaturated-saturated water flow
60 simulation. However, since the soil water flow is highly nonlinear in nature and
61 sensitive to atmospheric changes, soil utilizations, and human activities, the numerical
62 schemes require using fine discretization in vertical space and time for accurate
63 numerical solutions (Downer and Ogden, 2004; Varado et al., 2006). This makes the
64 numerical solutions computationally expensive, especially for large scale modeling
65 (Van Walsum and Groenendijk, 2008; Shen and Phanikumar, 2010; Yang et al., 2016;
66 Szymkiewicz et al., 2018). There are also many conceptual unsaturated-saturated water
67 flow models, e.g., SWAT (Arnold et al., 2012), INFIL 3.0 (Fill, 2008), HSPF (Duda et
68 al., 2012) and SALTMOD (Oosterbaan, 1998), which show advantages in mass balance
69 and computational cost. However, these models usually adopt many empirical

70 equations which result in poor performance comparing with the fully 3-D numerical
71 models.

72 To address the computational challenges discussed above, a variety of
73 simplifications have been introduced for the soil water flow for regional scale problems.
74 One simplification is to treat the hydrological processes (e.g., infiltration,
75 evapotranspiration, and deep percolation) occurring in the unsaturated zone as one-
76 dimensional (1-D) processes in the vertical direction. Field experiments at the regional
77 scale also show that, in the unsaturated zone, the lateral hydraulic gradient is usually
78 significantly smaller than the vertical gradient (Sherlock et al., 2002). This 1-D
79 simplification leads to the Quasi-3D scheme, which ignores the lateral flow in the
80 unsaturated zone but considers groundwater flow as a 3-D problem. The Quasi-3D
81 scheme avoids solving the 3-D Richards' equation for the unsaturated zone, and thus
82 improves computational efficiency and model stability. The Quasi-3D scheme is an
83 efficient solution for large-scale unsaturated-saturated flow modeling (Twarakavi, et al.,
84 2008; Yang et al., 2016) and is popular among groundwater modelers (Havard et al.,
85 1995; Harter and Hopmans, 2004; Graham and Butts, 2005; Stoppelenburg et al., 2005;
86 Seo et al., 2007; Markstrom et al., 2008; Ranatunga et al., 2008; Kuznetsov et al., 2012;
87 Xu et al., 2012; Zhu et al., 2012; Leterme et al., 2015). However, it is still challenging
88 when using the Quasi-3D models for a practical regional scale problem. Two concerns
89 arise as follows.

90 The first concern is the unsaturated modeling method. Although the Quasi-3D

scheme is computationally efficient, the numerical solutions of the 1-D Richards' equation still require intensive input data, and face numerical instability and mass balance errors under some specific situations (Zha et al., 2017). These problems limit their practical application for simulating regional scale problems under complicated geological and climate conditions as well as anthropogenic activities. As an alternative to the numerical solutions of the 1-D Richards' equation, water balance models have been used to describe soil water movements, which not only reduce the amount of input data but also improve computational efficiency and stability. The water balance models can be coupled with groundwater models. Facchi et al. (2004) coupled a conceptual soil water movement model SVAT with MODFLOW to simulate the hydrological relevant processes in the alluvial irrigated plains. Kim et al. (2008) integrated SWAT with MODFLOW to describe the exchange between hydrologic response units in the SWAT model and MODFLOW cells. The traditional water balance models however, may oversimplify soil water movement, and thus cannot accurately represent certain important features of soil water flow, e.g., the upward flux and soil heterogeneity. To extend the application of water balance model for more complicated conditions, Mao et al. (2018) developed a soil water balance model (called UBMOD model), which can simulate both upward and downward soil water movement in heterogeneous situation. And the model can be used with a coarse discretization in space and time, all of which make it suitable for the large-scale modeling.

Another concern is the scheme when coupling saturated models with unsaturated

models. There are three different numerical coupling schemes categorized by Furman (2008): uncoupled, iterative coupled, and fully coupled. The uncoupled scheme is widely used when using soil water flow packages with MODFLOW, such as LINKFLOW (Havard et al., 1995), SVAT-MODFLOW (Facchi et al., 2004), UZF1-MODFLOW (Niswonger et al., 2006), HYDRUS-MODFLOW (Seo et al., 2007), SWAP-MODFLOW (Xu et al., 2012). While this scheme is easy to be implemented, its results may not reliable when recharge from the unsaturated zone causes substantial changes of water table. Additionally, this scheme may result in the mass balance error (Shen and Phanikumar, 2010; Kuznetsov et al., 2012). The fully coupled scheme is mathematically and computationally rigorous, because it solves unsaturated and saturated flows simultaneously with internal boundary conditions of the two flows (Zhu et al., 2012). However, the fully coupled scheme is computationally expensive (Furman, 2008). The iterative coupled scheme offers a trade-off between model accuracy and computational cost (Yakirevich et al., 1998; Liang et al., 2003). And it has been widely used to couple two hydrodynamic models, both of which calculate the hydraulic head, and use the hydraulic head as the exchange information (Stoppelenburg et al., 2005; Kuznetsov et al., 2012). However, the soil water content is the variable calculated by soil water balance models other than the hydraulic head. Therefore, the traditional implementation method of the iterative scheme is inapplicability, and a specific implementation method of the iterative scheme should be developed to couple the soil water balance model and the hydrodynamic groundwater model.

In this study, a new Quasi-3D model is developed. The 1-D water balance model UBMOD developed by Mao et al. (2018) is integrated with MODFLOW (Harbaugh, 2005). A new implementation method of the iterative scheme is established for numerical solutions, and the net groundwater recharge and the depth of unsaturated zone (which is equal to the groundwater table depth) are chosen as the exchange information. The coupled model can achieve mass balance and keep numerical stability well, and it is suitable for large-scale modeling based on the characteristics of MODFLOW and UBMOD. Moreover, instead of developing a new package for MODFLOW, a framework of organizing the modeling procedures is developed. This paper elaborates the methodology of coupling the unsaturated and saturated water flow and the modeling framework in Sect. 2. Two published studies are used to test the performance of the coupled model when handling different water flow conditions in Sect. 3. A real-world application to study the regional net groundwater recharge is presented in Sect. 4.

2 Methodology and Model Development

In the new coupled model, the unsaturated-saturated domain is partitioned into a number of sub-areas in the horizontal direction mainly according to the spatially distributed inputs (soil types, atmosphere boundary conditions, land usage types, and crop types). A 1-D soil column is used to characterize the average soil water flow in each sub-area, and UBMOD is used to simulate the 1-D soil water flow. MODFLOW is used to simulate the 3-D groundwater flow of the whole domain. It is assumed that

154 the flow in the unsaturated zone is in the vertical direction, and that there is only vertical
155 exchange flux between the unsaturated and saturated zones. It is further assumed that
156 using the vertical column can reasonably simulate the unsaturated flow in each sub-area
157 while ignoring the horizontal heterogeneity. In this section, UBMOD is first presented,
158 followed by a brief introduction of MODFLOW and two peripheral tools (FloPy
159 (Bakker et al., 2016) and ArcPy (Toms, 2015)) used in the model. The procedures of
160 the new model and the modeling framework are described in Sect. 2.3, and the specific
161 implementation method of the unsaturated and saturated coupling scheme is described
162 in Sect. 2.4.

163 **2.1 The Soil Water Balance Model UBMOD**

164 This section describes the soil water balance model UBMOD to make this paper
165 self-contained, and more details of UBMOD are referred to Mao et al. (2018) or the
166 Appendix. The UBMOD is a water balance model based on a hybrid of numerical and
167 statistical methods. The model can effectively and efficiently simulate both downward
168 and upward soil water movement with only four physically meaning parameters, which
169 makes it suitable for practical application.

170 There are four major components to describe the soil water movement in UBMOD.
171 Firstly, the vertical soil column is divided into a cascade of "buckets" and each "bucket"
172 corresponds to a soil layer. The "buckets" will be filled to saturation from the top layer
173 to the bottom layer if there is infiltration, which is referred as the allocation of
174 infiltration water. Specifically speaking, the infiltration water first fills the top "bucket",

and then the excessive infiltration water moves downward to the next "bucket", until all the infiltration water is allocated in the "buckets". The governing equation of layer i is,

$$q_i = \min\left(M_i \times \left(\theta_{s,i} - \theta_i\right), I - I_{d,i-1}\right), \quad (1)$$

where i indicates the vertical soil layer, $i = 1, \ldots, j$; q_i is the amount of allocated water per unit area of layer i [L]; M_i is the thickness of layer i [L]; θ_i is the initial soil water content of layer i [L^3L^{-3}]; $\theta_{s,i}$ is the saturated soil water content of layer i [L^3L^{-3}]; I is the quantity of infiltration rate [L]; $I_{d,\,i-1}$ is the consumed infiltration water per unit area by all upper layers above layer i [L]. The infiltration rate I is an input data in the model, and the partitioning of rainfall between infiltration and runoff has not been considered by now.

Secondly, when the soil water content exceeds the field capacity, the soil water will move downward driven by the gravitational potential. The governing equation is,

$$\frac{\partial \theta}{\partial t} = -\frac{\partial K(\theta)}{\partial z}, \quad (2)$$

where t is the time [T]; z is the elevation in the vertical direction [L]. The vertical coordinate is positive downward. $K(\theta)$ is the unsaturated hydraulic conductivity [LT^{-1}] as a function of soil water content, which is characterized by empirical formulas referred to as drainage functions. The commonly used equations can be found in Mao et al. (2018) and the Appendix.

Thirdly, the source/sink terms are used to account for soil evaporation and crop transpiration. The governing equation is as follows,

$$\frac{\partial \theta}{\partial t} = -W, \tag{3}$$

where W is the source/sink term [T^{-1}]. The Penman-Monteith formula and Beer's law (also known as Ritchie-type equation) are adopted to estimate the potential soil evaporation E_p and potential crop transpiration T_p. Then E_p and T_p are distributed to each layer based on the evaporation cumulative distribution function and the root density function. The actual soil evaporation and crop transpiration are obtained by discounting E_p and T_p with the soil water stress coefficient.

Lastly, we calculate the diffusive movement driven by the matric potential. The governing equation is,

$$\frac{\partial \theta}{\partial t} = \frac{\partial}{\partial z}\left(D(\theta)\frac{\partial \theta}{\partial z} \right), \tag{4}$$

where $D(\theta)$ is the hydraulic diffusivity [L^2T^{-1}]. The finite difference method is used to solve the equation. An empirical formula with four parameters (saturated hydraulic conductivity K_s, saturated water content θ_s, field capacity θ_f, and residual water content θ_r) is used to describe the hydraulic diffusivity $D(\theta)$. The heterogeneity of soils is also taken into account by adding a correction item in the right side, which makes the model applicable to heterogeneous situations. With the help of the diffusive term, the UBMOD can consider upward soil water movement, which is ignored by most water balance models. The details of $D(\theta)$ are shown in the Appendix.

The original UBMOD is a soil water balance model, which cannot consider groundwater table. For the purpose of saturated-unsaturated coupling, the model has been improved to calculate the groundwater recharge, which is expatiated in Sect. 2.4.

2.2 The Brief Introduction of MODFLOW and Two Peripheral Tools

MODFLOW is a computer program that numerically solves the 3-D groundwater flow equation for a porous medium using a block-centered finite-difference method (Harbaugh, 2005). The governing equation solved by MODFLOW is,

$$\frac{\partial}{\partial x_i}\left(K_{ij}\frac{\partial H}{\partial x_j}\right)+W=S_s\frac{\partial H}{\partial t}, \quad (5)$$

where i, j = 1 - 3 indicate the x, y, and z directions, respectively; K_{ij} is the saturated hydraulic conductivity [LT^{-1}]; H is the hydraulic head [L]; W is the volumetric flux per unit volume representing sources and/or sinks of water [L^3T^{-1}]; S_s is the specific storage of the porous material [L^{-1}]; and t is the time [T].

FloPy and ArcPy are the two peripheral tools used in the model development. FloPy (Bakker et al., 2016) is a Python package for creating, running, and post-processing MODFLOW-based models. Unlike the commonly graphical user interfaces (GUIs) method, FloPy facilitates users to write a Python script to construct and post-process MODFLOW models, and it has been shown as a convenient and powerful tool by Bakker et al. (2016). Geographic information system (GIS) is a helpful tool for groundwater modeling by providing geospatial database and results presentation (Xu et al., 2011; Lachaal et al., 2012). ArcPy is an application program interface (API) of ArcGIS for Python (Toms, 2015), which provides a useful and productive way to perform geographic data analysis, data conversion, data management, and map automation with Python.

2.3 The Process of Geographic Input Information

238 The procedures of the modeling framework are composed of three major parts,
239 including the pre-processing, the coupled model, and the post-processing. The
240 preparation of geographic input information of the model shown in Fig. 1(a) is the major
241 component of pre-processing. The geographic information includes the domain area,
242 boundary conditions, sub-areas, digital elevation model (DEM), hydraulic conductivity
243 and porosity. The shapefile of the domain area (usually irregular in shape) is first
244 discretized by regular boundary with both active and inactive cells. The discretized
245 domain can be joined with the shapefile of boundary condition to generate the "ibound"
246 array of MODFLOW as shown in Fig. 1(a), which is used to specify which cells are
247 active, inactive, or fixed head in MODFLOW. The shapefile of sub-areas is joined with
248 the domain file, represented in subareas array with different number specified as
249 different sub-areas. The raster files of DEM, hydraulic conductivity and porosity are
250 further joined, and the values of these variables are listed in the arrays shown in Fig.1
251 (a). The unsaturated-saturated flow model coupling scheme will be described in next
252 section. The results presentations are accomplished by the post-processing tool, which
253 contains a series of utilities developed based on Python packages.

254 **2.4 Coupling Scheme of UBMOD and MODFLOW**

255 Figure 1(b) demonstrates the sketch map of the specific implementation method
256 of the unsaturated and saturated coupling scheme. The unsaturated-saturated domain is
257 partitioned into a number of sub-areas in the horizontal direction mainly according to
258 the spatially distributed inputs (each sub-area is considered to be homogeneous in

horizontal). There are *l* sub-areas, *j* layers for a specific soil column shown in Fig. 1(b). Soil water flow of each sub-area is simulated by using one 1-D soil column. The recharge at the bottom boundary calculated by UBMOD is treated as the upper boundary condition of MODFLOW. The whole saturated zone is discretized into a grid with cells, and there are *m* rows and *n* columns cells of the saturated zone as shown in Fig. 1(b). All cells in the same sub-area receive the same recharge from soil zone calculated by the representative 1-D soil column. In the vertical direction, both the saturated domain and the soil columns are discretized into different layers based on available data and information, and the layer discretization remain unchanged during the simulation. The lower boundary condition of the whole region is set in MODFLOW. As the soil water movement is reduced to 1-D flow, the surrounding boundary conditions for the unsaturated zone are no-flux boundary, while the surrounding boundary conditions for the saturated zone are set in MODFLOW as practical. Note that the saturated zone and the unsaturated zone are independent, but some layers may transform between the saturated zone and the unsaturated zone, which are referred as the overlap region. Fine vertical discretization of UBMOD in the overlap region is needed to improve the simulation accuracy.

Since the independent variable of UBMOD is the soil water content and the independent variable of MODFLOW is the hydraulic head, this study uses the vertical net recharge and the unsaturated zone depth to couple the unsaturated zone and saturated zone. The domain shown in Fig. 1(b) is used as an example to illustrate the

280 spatial and temporal coupling methods in the study. The vertical net recharge is
281 represented by vector **R** with $m \times n$ elements, and the unsaturated zone depth by vector
282 **Du** with l elements, as illustrated in Fig. 1(b). Scalar R is used to denote the specific net
283 recharge of a soil column to the corresponding saturated sub-area, and scalar d_u denotes
284 the depth of the soil column. Figure 2(a) shows the spatial coupling method of a soil
285 column connected with groundwater system. The water table locates in the j-th layer.
286 The net recharge R from soil zone is calculated by UBMOD as follows,

287 $$R = q_{\mathrm{I}} + q_{\mathrm{A}} + q_{\mathrm{S}} + q_{\mathrm{D}}, \tag{6}$$

288 where q_{I}, q_{A}, q_{S} and q_{D} are the fluxes across the water table caused by allocation of the
289 infiltration water, the advective movement driven by the gravitational potential,
290 source/sink terms and the water diffusion driven by the matric potential per unit area,
291 respectively [L].

292 These four terms are corresponded to the four major components in UBMOD, as
293 described in Sect. 2.1. Specifically, the infiltration water is allocated first according to
294 Eq. (1) if there is precipitation or irrigation. When there is residual infiltration water
295 across the water table in the j-th layer, the amount of residual infiltration is denoted as
296 q_{I}. Then the advective flow q_{A} across the water table driven by gravitational potential
297 is calculated by Eq. (2). The direction of these two terms is downward. The q_{S} term is
298 caused by evapotranspiration. When the critical depth of evapotranspiration is
299 shallower than the groundwater table depth, the groundwater can be consumed by
300 evapotranspiration and it causes an upward q_{S} term. A virtual layer is needed when

calculating the diffusive movement driven by matric potential across the water table based on Eq. (4). As shown in Fig. 2 (a), the virtual layer will be added under water table, numbered as layer j+1. The thickness, M_{j+1} [L], of the layer is set as,

$$M_{j+1} = z_{j+1} - d_u, \tag{7}$$

where z_{j+1} is the bottom depth of layer j+1 [L]; d_u is the thickness of unsaturated zone [L]. The amount of the upward flux between the virtual layer and layer j is denoted as q_D. Then, the net recharge matrix **R** for the whole area is obtained and used for the Recharge (RCH) package of MODFLOW.

The time coupling method is shown in Fig. 2(b). There are three levels of time discretization in the coupled model as follows: the stress period ΔT used in MODFLOW, the calculation time step for MODFLOW Δt_s, and the calculation time step for UBMOD Δt_u. The stress time step (ΔT) is also used in the iterative process, and the unsaturated model UBMOD and saturated model MODFLOW exchange information at the end of each stress period. Δt_u is a priori value and cannot be changed during the calculation. The UBMOD can give acceptable results when Δt_u is shorter than 10 d for assumed cases and 1 d for a real-world case (Mao et al., 2018). Δt_s is set as the technical report described by Harbaugh (2005) and can be changed during the calculation.

The implementation of iterative coupling scheme is shown in Fig. 2(c), which shows the calculation period from t to t+ΔT. At the time t, the saturated hydraulic head is known, marked as $\mathbf{H}^t$ ($m \times n$ dimension). When the model runs from t to t+ΔT, firstly, the initial saturated hydraulic head $\mathbf{H}^{t+\Delta T}$ at t+ΔT is set to be equal to $\mathbf{H}^t$, and then the

average unsaturated depth from t to $t+\Delta T$ is calculated according to $\mathbf{H}^{t+\Delta T}$, marked as $\mathbf{Du}^{t+\Delta T,\,p}$ (l elements). p is the iteration level. The $d_u^{t+\Delta T,p}$ for one soil column is calculated as follows,

$$d_u^{t+\Delta T,p} = \overline{D} - \overline{H^{t+\Delta T}}\ , \tag{8}$$

where $\overline{D}$ is the average depth from the soil surface to the impermeable layer of the controlling domain of the soil column [L]; $\overline{H^{t+\Delta T}}$ is the average thickness of controlling saturated domain of the soil column [L].

Secondly, the model runs UBMOD with the unsaturated time step Δt_u to obtain the vertical recharge at each time step (marked as r_t) until the time comes to be $t+\Delta T$. The total recharge during the stress period ΔT (from t to $t+\Delta T$) $R_{\Delta T}$ can be obtained by summarizing the recharge at each unsaturated time step, as follows,

$$R_{\Delta T} = \sum_{t}^{t+\Delta T} r_t\ , \tag{9}$$

The average recharge R from t to $t+\Delta T$ can be obtained by,

$$R = R_{\Delta T} / \Delta T\ . \tag{10}$$

Then the average recharge from all 1-D soil columns can be obtained, represented as $\mathbf{R}^{t+\Delta T,\,p}$, which is then used by the MODFLOW RCH package. Subsequently, the model runs the MODFLOW model with the saturated time step Δt_s to obtain the saturated hydraulic head until the time comes to $t+\Delta T$. The hydraulic head at the time $t+\Delta T$ is marked as $\mathbf{H}^{t+\Delta T,\,p}$ ($m\times n$ dimension). The convergence of the iteration is determined by using the difference of hydraulic head between the present $\mathbf{H}^{t+\Delta T,\,p}$ and the initial $\mathbf{H}^{t+\Delta T}$. The convergence criterion is,

$$if \quad \max\left(\left|\mathbf{H}^{t+\Delta T,p}-\mathbf{H}^{t+\Delta T}\right|\right)<\varepsilon_H, \tag{11}$$

where ε_H is a user-specified tolerance [L]. If the criterion is met, the iteration stops, and $\mathbf{H}^{t+\Delta T,p}$ is the convergent results at time $t+\Delta T$, and the model proceeds to the next stress period. Otherwise, the iteration continues to $p+1$ and $\mathbf{H}^{t+\Delta T,p}$ will be used to calculate the average unsaturated depth shown in Eq. (8). The above procedures will be repeated until the convergence criterion of Eq. (11) is met.

3 Model Evaluation

In this section, two test cases were designed to evaluate the model accuracy and the performance of the numerical coupling scheme under complicated soil and boundary conditions. The simulation results were compared with numerical results obtained using HYDRUS-1D (Šimůnek et al., 2008) and SWMS2D (Šimůnek et al., 1994), and with published experimental data. For these cases, the mean absolute relative error (*ARE*), the root mean squared error (*RMSE*), the index of agreement (*IA*) and the determination coefficient (R^2) are used to quantitatively evaluate the misfit between the simulated results of the coupled model and reference values, which are calculated as,

$$ARE=\frac{1}{x}\sum_{i=1}^{x}\frac{\left|y_i-Y_i\right|}{Y_i}\times 100\%, \tag{12}$$

$$RMSE=\sqrt{\frac{1}{x}\sum_{i=1}^{x}\left(Y_i-y_i\right)^2}, \tag{13}$$

$$IA=1-\frac{\sum_{i=1}^{x}\left(y_i-Y_i\right)^2}{\sum_{i=1}^{x}\left[\left|y_i-\bar{y}\right|+\left|Y_i-\bar{Y}\right|\right]^2}, \tag{14}$$

$$R^2 = 1 - \frac{\sum_{i=1}^{x}\left(y_i - Y_i\right)^2}{\sum_{i=1}^{x}\left(Y_i - \overline{Y}\right)^2}, \quad (15)$$

where the subscript i represents the serial number of the results; x represents the total number of the results; y_i is the simulated result of the coupled model and Y_i is the reference result; $\overline{y}$ is the average simulated result and $\overline{Y}$ is the average reference result.

3.1 Two Test Cases

3.1.1 Case 1: 1D upward flux with atmospheric condition

This case was to test the performance of the coupling scheme explained in Sect. 2.4. The case simulated a single field soil profile of the Hupselse Beek watershed in the Netherlands, which was used as a demo in HYDRUS-1D technical manual (Šimůnek, 2008). The soil profile consists of a 0.4 m-thick upper layer and a 1.9 m-thick bottom layer. The depth of the root zone is 0.3 m. The hydraulic parameters of the two soil layers are presented in Table 1. The surface boundary condition involves actual precipitation and potential transpiration rate as shown in Fig. 3. The groundwater level was initially set at 0.55 m below the soil surface. Only one vertical soil column and one MODFLOW cell were used in the coupled model. The parameters used in the coupled model are also listed in Table 1. The results from HYDRUS-1D were used as the reference of this test case. The stress period ΔT was set as 5 d, and the MODFLOW time step Δt_s and the UBMOD time step Δt_u were both set to be 1 d. The spatial discretization was 0.1 m.

To figure out the influence of the temporal and spatial discretization as well as the stress period on the simulation results, scenarios with different temporal and spatial resolution and the stress period of the coupled model were performed. Scenario 1 was set as the same as the above case. The UBMOD time step of scenario 2 and scenario 3 were 0.5 d and 2 d while other inputs were the same as scenario 1. The spatial discretization of scenario 4 and scenario 5 were set as 0.05 m and 0.2 m, while other inputs were the same as scenario 1. The stress period of scenario 6, scenario 7 and scenario 8 were set as 8 d, 10 d and 15 d while other inputs were the same as scenario 1. The 8 scenarios were marked as S1-S8.

3.1.2 Case 2: Two-dimensional (2-D) water table recharge experiment

This test case was used for model validation in a 2-D unsaturated-saturated flow system. The purpose of the case is to discuss the performance of the model under the condition with large lateral flux in the unsaturated zone. The numerical simulation of our model was compared with the data of a 2-D water table recharge experiment conducted by Vauclin et al. (1979). The experimental data have been used to test the variably saturated flow models (Clement et al., 1994) and coupled unsaturated-saturated flow models (Thoms et al., 2006; Twarakavi et al., 2008; Shen and Phanikumar, 2010; Xu et al., 2012). The 2-D domain is a rectangular sandy soil slab of 6.0 × 2.0 × 0.05 m. The initial pressure head is 0.65 m at the domain bottom. At the soil surface, a constant flux of q = 3.55 m/d is applied at the central 1.0 m, and the rest soil surface is the no flux boundary. Because of the symmetry of the flow system, only one

402 half of domain (right side) with the size of 3.0 m × 2.0 m × 0.05 was simulated. The
403 setup of the simulation is shown in Fig. 4(a). No-flow boundaries were defined on the
404 bottom and the left side, and specified hydraulic head boundary of 0.65 m was set on
405 the right side. The values of soil hydraulic parameters are listed in Table 1. The
406 simulation period is 8 h. In our coupled model, there were 30 uniform rectangular cells
407 used by MODFLOW, and there were 10 sub-areas defined to represent the unsaturated
408 zone, which were numbered from left to right. The first and last sub-areas covered 0.2
409 m and 0.4 m in the x direction respectively, and each of the rest sub-area covered 0.3 m
410 in the x direction. The first and the second sub-areas were used to define the recharge
411 boundary, while the other sub-areas were used to define the no-recharge boundary. The
412 stress period ΔT was set as 1 h, and the initial MODFLOW time step Δt_s and UBMOD
413 time steps Δt_u were set as 0.167 h. The spatial discretization of UBMOD was uniformly
414 0.1 m. The experiment was also simulated by using SWMS2D, which considered the
415 lateral flow. The mean time step of SWMS2D was set to be 0.0225 h, and 20, 200 finite
416 elements were used.

417 **3.2 Results and Discussions of Model Performance**

418 3.2.1 Computational accuracy of the coupling scheme

419 Figure 5 shows the comparison of the results simulated by HYDRUS-1D and the
420 coupled model of case 1. The statistical indexes are listed in Table 2. Figure 5(a)
421 demonstrates that the groundwater table depth calculated by the coupled model has a
422 similar pattern to that of HYDRUS-1D. The *ARE*, *RMSE*, *IA* and R^2 values were 17.0%,

0.171 m, 0.976 and 0.977. The soil water contents at the depth of 1.15m over time from the two models are compared in Fig. 5(b). The *ARE*, *RMSE*, *IA* and R^2 were 2.2%, 0.008 cm^3/cm^3, 0.991 and 0.976. The simulated soil water content profiles at different times are shown in Fig. 5(c)-(e) and the evaluation indexes demonstrate the satisfactory performance of the model. Moreover, the net groundwater consumption at the end of the simulation period was compared, which is 0.132 m calculated by the coupled model, and it is the same with that from HYDRUS-1D. In general, these results indicate that the coupled model can capture the flow information under the upward flux and the heterogeneous condition.

The deviations of groundwater table depth and soil water content from the coupled model and HYDRUS-1D can also be observed in Fig. 5. The deviations are caused by the different model structures of the coupled model and HYDRUS-1D. The HYDRUS-1D solves the saturated-unsaturated flow together, and the groundwater table is determined at the depth with the matric potential equaling to zero. The soil water content of the capillary fringe above the groundwater table is almost saturated. However, the UBMOD model cannot simulate the capillary fringe. And there is a parameter the field capacity used to calculate the downward movement of soil water, which is defined under a free drainage condition. So, the coupled model could lead to the lower soil water content in the capillary fringe and higher groundwater table as shown in Fig. 5. And there is another parameter specific yield used in the coupled model to determine the groundwater table, which also attributes to the deviation of groundwater table.

Figure 4(b) shows the comparison of simulated water tables at 4 different times using the coupled model and SWMS2D and the observation data in case 2. The index values are listed in Table 3. The coupled model matched the observation data well at the simulation times of 3 h, 4 h and 8 h, with the *ARE* values smaller than 3%, the *RMSE* values smaller than 0.03 m and the *IA* and R^2 values close to 1. The observed and simulated soil water content profiles for the initial and ending times are presented in Fig. 6. The statistical index values are also listed in Table 3. The simulations by the coupled model agree well with the observations at the locations of x = 0.2 m, x = 1.4 m and x = 2 m (Figs. 6(a), (d) and (e)) where the lateral water flow is negligible. The calculated recharge is 3.55 m/d per unit area when the flow becomes steady, which equals to the input flux. These results demonstrate the accuracy of the coupled model and the reliability of the coupling scheme shown in Sect. 2.4.

3.2.2 Influence of the temporal and spatial discretization as well as the stress period on simulation results

The groundwater table depth calculated by scenarios with different temporal discretizations (S1-S3) are compared with those from HYDRUS-1D in Fig. 7(a). The statistical index values are shown in Table 2. It can be found that the water table depth calculated by different scenarios have the same variation trend. The *ARE* values of the three scenarios are smaller than 20%, and the maximum *RMSE* value is 0.171 m. The *IA* and R^2 values are larger than 0.95. The groundwater table depth calculated by scenarios with different spatial discretizations (S1, S4 and S5) are compared with those

from HYDRUS-1D in Fig. 7(b). The *ARE* values of the three scenarios are smaller than 25%. The maximum *RMSE* value is 0.215 m. The *IA* and R^2 values are larger than 0.95. The water table depth calculated by scenarios with different stress periods (S1, S6, S7 and S8) are compared with those from HYDRUS-1D in Fig. 7(c). It should be noted that the model collapsed at the time of 227 d when the stress period is 15 d (S8). The statistical index values for S1, S6 and S7 are shown in Table 2. The *ARE* and *RMSE* values of the three scenarios are very similar. Considering the water balance method and empirical formulas adopting in the coupled model, the results calculated by all the scenarios except S8 are acceptable. These results indicate that the temporal and spatial discretization have slight influence on the modeling results. It should be noted that the impact of stress period in a certain scale (<10 d in this case) has no significant impact on the simulation results. However, a too large stress period will cause improper results.

3.2.3 Limitations of the coupled model

Although the coupled model had a sufficient computational accuracy as shown above, there were limitations because of the Quasi-3D assumptions. The coupled model overestimates the water table at the time of 2 h in case 2 as shown in Fig. 4(b). This is caused by a significant lateral flow in the unsaturated zone during the early period due to the relatively low initial soil water content condition. Therefore, a portion of the infiltration water in the first and second sub-areas should move in the lateral direction, instead of moving downward to the saturated zone as in the Quasi-3D model. The coupled model thus overestimates the recharge flux, and results in a higher water table

at the early period. Additionally, the simulated soil water content by the coupled model has poor performance at the locations of x = 0.6 m and x = 0.8 m (Fig. 6(b) and (c)). These two sub-areas are close to the recharge zone and affected by the lateral flow, which is ignored in the coupled model. These phenomena are similar to the results calculated by other Quasi-3D models (Xu et al., 2012; Shen and Phanikumar, 2010). Therefore, the coupled model overestimates the recharge and underestimates the soil water content when the lateral flow cannot be ignored. Its application should be limited to cases in which the soil flow mainly occurs in the vertical direction.

3.2.4 Water mass balance and computational cost

The mass balance error of the coupled model is small with the maximum value 0.012% in case 1 and 0.004% in case 2, while they are 1.6% for the HYDRUS-1D model and 0.133% for the SWMS2D model. The cases were run on a 6 GB RAM, double 2.93 GHz intel Core (TM) 2 Duo CPU-based personal computer. The computational cost of different scenarios in case 1 of the coupled model ranges from 49 s to 63 s as listed in Table 2. It is 1.4 s by HYDRUS-1D. The temporal and spatial discretization has slight influence on computational cost, while the stress period has significant influence on the computation cost. The iteration and information exchange are responsible for the high computational cost. For case 2, the computational cost of the coupled model and the SWMS2D model are 46 s and 95 s, respectively. The coupled model has a better efficiency comparing with the complete 2D model due to its simpler numerical solutions and coarse discretization in space and time. The advantage of

507 descreasing computational cost will be more obvious when the application scale
508 becomes larger. Generally speaking, the coupled model provides satisfactory mass
509 balance and good computational efficiency.

510 **4 Real-World Application**

511 **4.1 Study Site and Input Data**

512 The coupled model was used to calculate the regional-scale groundwater recharge
513 in a real-world case, where the shallow groundwater has significant impact on the soil
514 water movement. Figure 8(a) shows the location of the study site, the Yonglian
515 irrigation area (107°37′19″ - 108°51′04″ E, 40°45′57″ - 41°17′58″ N) in Inner Mongalia,
516 China. The irrigation area is 12 km long from north to south, and 3 km wide from east
517 to west. The whole domain size is 29.75 km^2. The ground surface elevation decreases
518 from 1028.9 m to 1025.4 m from the southwest to the northeast. A two-year tracer
519 experiment from 2014 to 2016 was conducted to obtain the groundwater recharge (Yang,
520 2018), and the experimental locations are shown in Fig. 8(a). This irrigation area has
521 well-defined hydrogeological borders by the channel network. Since the Zaohuo Trunk
522 Canal and No. 6 Drainage Ditch are filled with water over the simulation time, the first-
523 kind boundary condition was applied to the two segments. The non-flow boundary
524 condition was used for the other segments. The irrigation water of this area is diverted
525 from the Renmin Canal. This irrigation area was divided into three sub-areas according
526 to the land usage since they own significantly different upper boundary conditions,
527 which are farm land, villages and bared soil, as shown in Fig. 8(b). The crop types in

528 the farmland were not considered for determining the sub-areas. The surface digital
529 elevation model (DEM) is shown in Fig. 8(c).
530 The measured soil water content and groundwater table in the crop growing season
531 from May to October of 2004 were used to calibrate the hydraulic parameters, and the
532 tracer experiment from 2014 to 2016 was used for the groundwater recharge evaluation.
533 A uniform daily rainfall rate was applied to the whole domain. The irrigation water was
534 only applied to the farm land. As lack of the weather data in 2004, the potential
535 evapotranspiration ET_0 was calculated by the measured evaporation data from the 20
536 cm pan (ET_{20}), multiplying by an empirical conversion coefficient. The empirical
537 coefficient is 0.55, which was recommended by Hao (2016) by comparing monthly ET_0
538 and ET_{20} with 8 years' data in this area. The ET_0 during 2014 to 2016 was calculated
539 by using the Penman-Monteith equation. The precipitation, irrigation and ET_0 are
540 shown in Fig. 9. The crop growing season is from May to October, and the rest months
541 are no-crop growing season. Based on the hydrogeological characteristics of the study
542 area provided by the Geological Department of Inner Mongolia, the top aquifer within
543 the depth of 7 m is loamy sand and loam with small hydraulic conductivity; an
544 underlying sand aquifer with the thickness of 46 m has high permeability, and the sand
545 aquifer is lying on an impervious 1 m-thick clay layer. The clay layer was used as the
546 bottom of the simulation domain, and seven different geological layers were used in the
547 MODFLOW model. The first layer was set to be the top aquifer, and the second aquifer
548 were divided into 6 layers for numerical simulation. Ten groundwater monitoring wells

549 were set in this district, and the groundwater tables were observed every 6 days. Well
550 1, well 2, well 3, well 5 and well 6 are located in farm land areas, well 4 and well 8 in
551 villages, and well 7, well 9 and well 10 in bared soil areas. Additionally, there are 5 soil
552 water content monitoring points in the farm land and 2 points in the bared soil area, as
553 shown in Fig. 8(a). Soil water contents within 1 m depth were observed 1-3 times every
554 month from May to October in 2004.

555 Five GIS files are prepared as the shapefile files of the study domain, the land
556 usage types, the boundary conditions, and raster files of the surface DEM and initial
557 hydraulic head. There were 150 rows and 50 columns used in the MODFLOW model.
558 The spatial discretization of UBMOD was set to be 0.1 m. The stress period ΔT was set
559 as 5 d, and the MODFLOW time step Δt_s and UBMOD time step Δt_u were set as 1 d.

560 **4.2 Model Calibration Results**

561 There are two soil types in the first layer as loamy sand and loam. The unsaturated
562 hydraulic parameters of the two soils are listed in Table 4. The hydraulic conductivity
563 of the top aquifer in MODFLOW was set as the same as the unsaturated layer, and the
564 hydraulic conductivity of the bottom sand aquifer was set as 3.5 m/d during the
565 calibration, and the specific yields of the top and bottom were set as 0.08 and 0.1,
566 respectively. Figure 10 shows the comparison of the simulated and observed water table
567 depth for the whole area and locations of different monitoring wells. The statistical
568 index values are listed in Table 5. It can be found that the *ARE*, *RMSE*, *IA* and R^2 values
569 are 9.9%, 0.203 m, 0.869 and 0.71 for the regional average water table depth. Larger

570 deviations of simulated water table depth can be found for the locations of monitoring
571 wells, with *RMSE* values ranging from 0.25 m-0.39 m. Figure 11 further shows the
572 spatial distribution of the simulated water table depth at different output times. The
573 increasing trend is obviously found in Fig. 11(a) to Fig. 11(c) in the crop growing season,
574 during which the groundwater was consumed by crop transpiration and strong soil
575 evaporation. When the intensive autumn irrigation happened after the 160^{th} day, the
576 water table depth in the farm land decreased rapidly, as shown in Fig. 11(d). These
577 results indicate that our model can reasonably simulate the water table depth trend in
578 space and time.

579 The recharge during short-term was calculated for further checking the results by
580 comparing the results with those from reference papers. The calculated recharge in farm
581 land during the autumn irrigation (from Oct 16 to Oct 31) is 93.3 mm, and the
582 coefficient of recharge from the autumn irrigation is 0.37. Zhang (2011) proposed the
583 coefficient of recharge from the autumn irrigation is approximately 0.3. Yang (2016)
584 proposed that the coefficient of the recharge from the autumn irrigation is between 0.36
585 and 0.4. Yu (2017) used the coefficient of recharge from autumn irrigation as 0.33 for
586 the district. The calculated result is consistent with the previous studies. The phreatic
587 evaporation coefficient was estimated during the period from Sep 15 to Sep 30 with no
588 precipitation or irrigation. The quantity of the recharge from saturated zone to
589 unsaturated zone is 10.1 mm during the period in the farm land. The phreatic
590 evaporation coefficient is 0.179, and the averaged water table depth is 1.51 m during

591 the period. The phreatic evaporation coefficient measured by Wang (2002) is 0.172 at
592 the depth of 1.5 m. The short-term results indicate the validity of the simulating results.
593 Figure 12 shows the comparison between the simulated and average observed soil
594 water content profiles of the farm land and bared soil at different times. The statistical
595 index values are listed in Table 5. The *ARE* values of the farm land at the times of 40d,
596 85d, 125d, and 166d are 15.3%-24.9%, the *RMSE* values 0.044 cm^3/cm^3- 0.066 cm^3/cm^3,
597 the *IA* values 0.621-0.775, and the R^2 values 0.54-0.689. The corresponding values for
598 the bared soil are 10.8%-19.8%, 0.038 cm^3/cm^3-0.052 cm^3/cm^3, 0.823-0.905, 0.620-
599 0.813, respectively. The larger measured soil water content in the root zone for the farm
600 land can be observed than the simulations, while the simulated soil water content
601 profiles in the bared soil agree well with the observations, as shown in Fig. 12. The
602 reason may be that the sampling locations are at the border of fields, which leads to an
603 overestimation of the soil water content in the root zone due to smaller crop root uptake.
604 The computational cost of the real-world application is 120 s, which is efficient
605 considering the scale of the problem.
606 **4.3 Regional Groundwater Recharge**
607 In the tracer experiment, bromide (Br) was used as the tracer for calculating
608 groundwater recharge. The tracer was injected at 1 m depth at two locations shown in
609 Fig. 8(a) in October, 2014. Based on two sampling locations in October of 2015 and
610 2016, the downward recharge is estimated according to the movement distance of the
611 tracer peak and the average water content from the initial position of the tracer to the

612 final position (Tan et al., 2014). The soil water content at the depth of 1 m is relatively
613 stable according to the measurements and the results of Peng (2015), which ensures the
614 reliability of the experiment. As shown in Table 6, the annual average recharge *R* is 33.8
615 mm/year, and the recharge coefficient is 0.055 during the period of 2014 - 2016.

616 The calibrated coupled model was used to estimate the groundwater recharge from
617 October 1, 2014 to September 30, 2016. Figure 13 shows the time series of simulated
618 recharge rate in the farm land, and Table 6 lists the simulation results. The simulation
619 results indicate that groundwater is recharged in the no-crop growing season and
620 consumed in the crop growing season. The two peak values of groundwater recharge in
621 Fig. 13 are due to the autumn irrigation after harvest for washing salt out. The no-crop
622 growing season provides 92.30 mm/year groundwater recharge over a year and the
623 average recharge coefficient is 0.346, which indicates that the autumn irrigation in the
624 no-crop growing season provides the primary groundwater recharge in the year. In the
625 crop growth season, the recharge is negative, which means that groundwater is
626 consumed by crop transpiration and soil evaporation. As calculated by the coupled
627 model, the annual groundwater recharge is 36.21 mm/year during the period from
628 October 1, 2014 to September 30, 2016 in the farm land, which is similar to the result
629 of the tracer experiment. The results confirm the coupled model for groundwater
630 recharge evaluation, which is helpful for scheduling the irrigation amount in the crop
631 growing season under the water saving policies.

632 **5 Conclusions**

This study developed a new Quasi-3D coupled model for the purpose of practical modeling of unsaturated-saturated flow at the regional scale. The 1-D water balance model UBMOD describing the unsaturated soil water flow was integrated with MODFLOW iteratively. A developed framework implemented the modeling procedures, and provided the pre- and post-processing tools. The model was evaluated by using both synthetic numerical examples and real-world experimental data. The major conclusions drawn from this research are as follows,

(1) The new iteration coupling scheme iteratively integrating a hydrodynamic model with a water balance model is reliable. The vertical net recharge and the depth of the unsaturated zone are effective to be used as the exchange information to couple the unsaturated zone and saturated zone.

(2) The satisfactory results in the two testing examples demonstrate the effectiveness of the new Quasi-3D model with an acceptable calculative efficiency and well-maintained saturated zone and unsaturated zone mass balance.

(3) The spatial and temporal discretization has slight impact on the simulation results. The stress period should be not too large and it also has slight impact on the simulation results in a certain range.

(4) The model gives a satisfactory performance for calculating the groundwater recharge measured from the tracer experiment. The calculated annual groundwater recharge is 36.21 mm/year and the recharge coefficient is 0.059 in the study area.

(5) The coupled model should not be used for problems with substantial lateral flow in

the unsaturated zone because of the Quasi-3D assumptions used in the model.

(6) The coupled model could lead to a higher groundwater table depth since it ignores the capillary fringe.

Acknowledgments

The study was supported by Natural Science Foundation of China through Grants 51790532, 51779178, and 51629901. Requests for data not explicitly provided in the manuscript may be made to the corresponding author.

References

Arnold, J., Moriasi, D., Gassman, P., Abbaspour, K., White, M., Srinivasan, R., Santhi, C., Harmel, R., van Griensven, A., Van Liew, M., Kannan, N., Jha, M.: SWAT: model use, calibration, and validation, Trans. ASABE., 55 (4), 1491-1508, doi: 10.13031/2013.42256, 2012.

Bakker, M., Post, V., Langevin, C., Hughes, J., White, J., Starn, J. and Fienen, M.: Scripting MODFLOW model development using Python and FloPy, Groundwater, 54(5), 733-739, doi:10.1111/gwat.12413, 2016.

Bouwer, H.: Integrated water management: emerging issues and challenges, Agric. Water Manage., 45(3), 217-228, doi:10.1016/S0378-3774(00)00092-5, 2000.

Brunner, P. and Simmons, C.: HydroGeoSphere: a fully integrated, physically based hydrological model, Groundwater, 50(2), 170-176, doi:10.1111/j.1745-6584.2011.00882.x, 2012.

675 Clement, T., Wise, W. and Molz, F.: A physically based, two-dimensional, finite-
676 difference algorithm for modeling variably saturated flow, J. Hydrol., 161(1-4),
677 71-90, doi:10.1016/0022-1694(94)90121-X, 1994.
678 Diersch, H.: FEFLOW: finite element modeling of flow, mass and heat transport in
679 porous and fractured media, Springer Science & Business Media, Berlin, German,
680 2013.
681 Downer, C. and Ogden, F.: Appropriate vertical discretization of Richards' equation for
682 two-dimensional watershed-scale modelling, Hydrol. Process., 18(1), 1-22,
683 doi:10.1002/hyp.1306, 2004.
684 Duda, P., Hummel, P., Donigian Jr, A., Imhoff, J.: BASINS/HSPF: model use,
685 calibration, and validation, Trans. ASABE., 55(4), 1523-1547, doi:
686 10.13031/2013.42261, 2012.
687 Evans, R. and Sadler, E.: Methods and technologies to improve efficiency of water use,
688 Water Resour. Res., 44(7), doi:10.1029/2007WR006200, 2008.
689 Facchi, A., Ortuani, B., Maggi, D. and Gandolfi, C.: Coupled SVAT–groundwater
690 model for water resources simulation in irrigated alluvial plains, Environ. Modell.
691 Softw., 19(11), 1053-1063, doi:10.1016/j.envsoft.2003.11.008, 2004.
692 FILL, V.: Documentation of Computer Program INFIL3.0-A Distributed-Parameter
693 Watershed Model to Estimate Net Infiltration Below the Root Zone, U.S.
694 Geological Survey, Virginia, U.S., 2008.
695 Furman, A.: Modeling coupled surface-subsurface flow processes: a review, Vadose

696 Zone J., 7(2), 741-756, doi:10.2136/vzj2007.0065, 2008.
697 Graham, D. and Butts, M.: Flexible, integrated watershed modelling with MIKE SHE,
698 in: Watershed Models, edited by: Singh, V., and Frevert, D., CRC Press, Cleveland,
699 Ohio, U.S., 2005.
700 Hao, P.: Regional soil water-salt balance in Hetao Irrigation District with drip irrigation
701 and combined use of surface water and groundwater, Master thesis, School of
702 Water Resources and Hydropower Engineering, Wuhan University, China, 2016.
703 Harbaugh, A.: MODFLOW-2005, the U.S. Geological Survey modular ground-water
704 model -- the Ground-Water Flow Process, U.S. Geological Survey, Virginia, U.S.,
705 2005.
706 Harter, T. and Hopmans, J.: Role of vadose zone flow processes in regional scale
707 hydrology: Review, opportunities and challenges, In: Unsaturated Zone Modeling:
708 Progress, Challenges and Applications, editor by: Feddes, R., de Rooij, G., van
709 Dam, J., Kluwer Academic Publishers, Dordrecht, Netherlands, 179–210, 2004.
710 Havard, P., Prasher, S., Bonnell, R. and Madani, A.: Linkflow, a water flow computer
711 model for water table management: Part I. Model development, T. ASABE., 38(2),
712 481-488, doi:10.13031/2013.27856, 1995.
713 Karandish, F., Salari, S. and Darzi-Naftchali, A.: Application of virtual water trade to
714 evaluate cropping pattern in arid regions, Water Resour. Manage., 29(11), 4061-
715 4074, doi:10.1007/s11269-015-1045-4, 2015.
716 Kim, N., Chung, I., Won, Y. and Arnold, J.: Development and application of the

integrated SWAT–MODFLOW model, J. Hydrol., 356(1-2): 1-16, doi:10.1016/j.jhydrol.2008.02.024, 2008.

Kuznetsov, M., Yakirevich, A., Pachepsky, Y., Sorek, S. and Weisbrod, N.: Quasi 3D modeling of water flow in vadose zone and groundwater, J. Hydrol., 450, 140-149, doi:10.1016/j.jhydrol.2012.05.025, 2012.

Lachaal, F., Mlayah, A., Bédir, M., Tarhouni, J. and Leduc, C.: Implementation of a 3-D groundwater flow model in a semi-arid region using MODFLOW and GIS tools: The Zéramdine–Béni Hassen Miocene aquifer system (east-central Tunisia), COMPUT. GEOSCI-UK., 48, 187-198, doi:10.1016/j.cageo.2012.05.007, 2012.

Leterme, B., Gedeon, M., Laloy, E. and Rogiers, B.: Unsaturated flow modeling with HYDRUS and UZF: calibration and intercomparison. In: MODFLOW and More 2015, Golden, CO, Integrated GroundWater Modeling Center, 2015.

Liang, X., Xie, Z. and Huang, M.: A new parameterization for surface and groundwater interactions and its impact on water budgets with the variable infiltration capacity (VIC) land surface model, J. Geophys. Res-Atmos., 108(D16), doi:10.1029/2002JD003090, 2003.

Mao, W., Yang, J. Zhu, Y., Ye, M., Liu, Z. and Wu, J.: An efficient soil water balance model based on hybrid numerical and statistical methods, J. Hydrol., 559, 721-735, doi:10.1016/j.jhydrol.2018.02.074, 2018.

Markstrom, S., Niswonger, R., Regan, R., Prudic, D. and Barlow, P.: GSFLOW-Coupled Ground-water and Surface-water FLOW model based on the integration

738 of the Precipitation-Runoff Modeling System (PRMS) and the Modular Ground-
739 Water Flow Model (MODFLOW-2005), U.S. Geological Survey, Virginia, U.S.,
740 2008.
741 Niswonger, R., Prudic, D. and Regan, R.: Documentation of the Unsaturated-Zone
742 Flow (UZF1) Package for modeling unsaturated flow between the land surface and
743 the water table with MODFLOW-2005, U.S. Geological Survey, Virginia, U.S.,
744 2006.
745 Oosterbaan, R.: SALTMOD: Description of Principles and Application, ILRI,
746 Wageningen, 1998.
747 Peng, Z.Y.: Mechanism and modeling of coupled water-heat-solute movement in
748 unidirectional freezing soils, Doctor thesis, School of Water Resources and
749 Hydropower Engineering, Wuhan University, China, 2015.
750 Ranatunga, K., Nation, E. and Barratt, D.: Review of soil water models and their
751 applications in Australia, Environ. Modell. Softw., 23(9), 1182-1206,
752 doi:10.1016/j.envsoft.2008.02.003, 2008.
753 Seo, H., Šimůnek, J. and Poeter, E.: Documentation of the hydrus package for
754 MODFLOW-2000, the us geological survey modular ground-water model,
755 IGWMC-International Ground Water Modeling Center, U.S., 2007.
756 Shen, C. and Phanikumar, M.: A process-based, distributed hydrologic model based on
757 a large-scale method for surface-subsurface coupling, Adv. Water Resour., 33(12),
758 1524-1541, doi:10.1016/j.advwatres.2010.09.002, 2010.

759 Sherlock, M., McDonnell, J., Curry, D. and Zumbuhl, A.: Physical controls on septic
760 leachate movement in the vadose zone at the hillslope scale, Putnam County, New
761 York, USA, Hydrol. Preocess., 16(13), 2559-2575, doi:10.1002/hyp.1048, 2002.
762 Šimůnek, J., van Genuchten, M. T. and Šejna, M.: HYDRUS: Model use, calibration
763 and validation, T. ASABE., 55(4), 1261-1274, doi:10.13031/2013.42239, 2012.
764 Šimůnek, J., Šejna, M., Saito, H., Sakai, M. and van Genuchten, M. T.: The HYDRUS-
765 1D Software Package for Simulating the Movement of Water, Heat, and Multiple
766 Solutes in Variably Saturated Media, Version 4.0, HYDRUS Software Series 3,
767 Department of Environmental Sciences, University of California Riverside,
768 Riverside, California, U.S., 2008.
769 Šimůnek, J., Vogel, T. and van Genuchten, M. T.: The SWMS_2D code for simulating
770 water flow and solute transport in two-dimensional variably saturated media,
771 Research Report, California, U.S., 1994.
772 Sophocleous, M.: Groundwater recharge and sustainability in the High Plains aquifer
773 in Kansas, USA, Hydrogeol. J., 13(2), 351-365, doi:10.1007/s10040-004-0385-6,
774 2005.
775 Stoppelenburg, F., Kovar, K., Pastoors, M. and Tiktak, A.: Modelling the interactions
776 between transient saturated and unsaturated groundwater flow, RIVM report
777 500026001, 2005.
778 Szymkiewicz, A., Gumuła-Kawęcka, A., Šimůnek, J., Leterme, B., Beegum, S.,
779 Jaworska-Szulc, B., Pruszkowska-Caceres, M., Gorczewska-Langner, W.,

Angulo-Jaramillo, R. and Jacques, D.: Simulations of freshwater lens recharge and salt/freshwater interfaces using the HYDRUS and SWI2 packages for MODFLOW, J. Hydrol. Hydromech., 66(2), 246-256, doi: 10.2478/johh-2018-0005, 2018.

Tan, X., Wu, J., Cai, S. and Yang, J.: Characteristics of groundwater recharge on the North China Plain. Groundwater, 52(5), 798-807, doi:10.1111/gwat.12114, 2014.

Thoms, R., Johnson, R. and Healy, R.: User's guide to the variably saturated flow (VSF) process for MODFLOW. U.S. Geological Survey Techniques and Methods 6-A18, Virginia, U.S., 2006.

Tian, Y., Zheng, Y., Wu, B., Wu, X., Liu, J. and Zheng, C.: Modeling surface water-groundwater interaction in arid and semi-arid regions with intensive agriculture, Environ. Modell. Softw., 63, 170-184, doi:10.1016/j.envsoft.2014.10.011, 2015.

Toms. S.: ArcPy and ArcGIS-Geospatial Analysis with Python, Packt Publishing Ltd, Birmingham, UK, 2015.

Twarakavi, N., Šimůnek, J. and Seo, H.: Evaluating interactions between groundwater and vadose zone using the HYDRUS-based flow package for MODFLOW, Vadose Zone J., 7(2), 757-768, doi:10.2136/vzj2007.0082, 2008.

Van Walsum, P. and Groenendijk, P.: Quasi steady-state simulation of the unsaturated zone in groundwater modeling of lowland regions, Vadose Zone J., 7(2), 769-781, doi:10.2136/vzj2007.0146, 2008.

VanderKwaak, J. and Loague, K.: Hydrologic‐response simulations for the R‐5

801 catchment with a comprehensive physics‐based model, Water Resour. Res.,
802 37(4), 999-1013, doi:10.1029/2000WR900272, 2001.
803 Varado, N., Ross, P. and Haverkamp, R.: Assessment of an efficient numerical solution
804 of the 1D Richards equation on bare soil, J. Hydrol., 323(1-4), 244-257,
805 doi:10.1016/j.jhydrol.2005.07.052, 2006.
806 Vauclin, M., Khanji, J. and Vachaud, G.: Experimental and numerical study of a
807 transient, two-dimensional unsaturated-saturated water table recharge problem,
808 Water Resour. Res., 15(5), 1089-1101, doi:10.1029/WR015i005p01089, 1979.
809 Wang, W., Zhang, Z., Yeh, T., Qiao, G., Wang, W., Duan, L., Huang, S. and Wen, J.:
810 Flow dynamics in vadose zones with and without vegeration in an arid region, Adv.
811 Water Resour., 106, 68-79, doi:10.1016/j.advwatres.2017.03.011, 2017.
812 Wang, Y.: The analysis of the regional scale groundwater table variation before and
813 after the water-saving transformation in Hetao Irrigation District, Water Saving
814 Irrigation, 01, 15-17, 2002.
815 Weill, S., Mouche, E. and Patin, J.: A generalized Richards equation for
816 surface/subsurface flow modeling, J. Hydrol., 336(1-4), 9-20,
817 doi:10.1016/j.jhydrol.2008.12.007, 2009.
818 Xu, X., Huang, G., Qu, Z. and Pereira, L.: Using MODFLOW and GIS to access
819 changes in groundwater dynamics in response to water saving measures in
820 irrigation districts of the upper Yellow River basin, Water Resour. Manage., 25(8),
821 2035-2059, doi:10.1007/s11269-011-9793-2, 2011.

822 Xu, X., Huang, G., Zhan, H., Qu, Z. and Huang, Q.: Integration of SWAP and
823 MODFLOW-2000 for modeling groundwater dynamics in shallow water table
824 areas, J. Hydrol., 412, 170-181, doi:10.1016/j.jhydrol.2011.07.002, 2012.
825 Yakirevich, A., Borisov, V. and Sorek, S.: A quasi three-dimensional model for flow
826 and transport in unsaturated and saturated zones: 1. Implementation of the quasi
827 two-dimensional case, Adv. Water Resour., 21(8), 679-689, doi:10.1016/S0309-
828 1708(97)00031-6, 1998.
829 Yang, J., Zhu, Y., Zha, Y. and Cai, S.: Mathematical model and numerical method of
830 groundwater and soil water movement, Science press, Beijing, China, 2016.
831 Yang, W.: Numerical simulation of conjunctive use of groundwater and surface water
832 in Yongji Irrigation Field of Hetao Irrigation District, Master thesis, School of
833 Water Resources and Hydropower Engineering, Wuhan University, China, 2016.
834 Yang, X.: Soil salt balance in Hetao Irrigation District based on the SaltMod and tracer
835 experiment, Master thesis, School of Water Resources and Hydropower
836 Engineering, Wuhan University, China, 2018.
837 Yu. L.: Numerical simulation of conjunctive use of groundwater and surface water in
838 Hetao Irrigation District and water resources forecase, Master thesis, School of
839 Water Resouces and Hydropower Engineering, Wuhan Univerisity, China, 2017.
840 Zha, Y., Yang, J., Yin, L., Zhang, Y., Zeng, W. and Shi, L.: A modified Picard iteration
841 scheme for overcoming numerical difficulties of simulating infiltration into dry
842 soil, J. Hydrol. 551, 56-69, doi:10.1016/j.jhydrol.2017.05.053, 2017.

Zhang, J., Zhu, Y., Zhang, X., Ye, M. and Yang, J.: Developing a long short-term memory (LSTM) based model for predicting water table depth in agricultural areas, J. Hydrol., 561, 918-929, doi:10.1016/j.jhydrol.2018.04.065, 2018.

Zhang, Z.: Irrigation infiltration and recharge coefficient in Hetao Irrigation District and the primary study on threshold value of water in different diversion, Master thesis, Inner Mongolia Agricultural University, China, 2011.

Zhu, Y., Shi, L., Lin, L., Yang, J. and Ye, M.: A fully coupled numerical modeling for regional unsaturated-saturated water flow, J. Hydrol., 475(12), 188-203, doi:0.1016/j.jhydrol.2012.09.048, 2012.

853 LIST OF TABLES

854 Table 1. The hydraulic parameters of case 1 and case 2.

	Depth (m)	The parameters used by HYDRUS-1D/SWMS2D and the coupled model			The parameters used only by HYDRUS-1D/SWMS2D		The parameters used only by the coupled model	
		θ_r (-)	θ_s (-)	K_s (m/d)	n	α (1/m)	θ_f (-)	μ
Case 1	0-0.4	0.001	0.399	0.2975	1.3757	1.74	0.25	-
	0.4-2.3	0.001	0.339	0.4534	1.6024	1.39	0.23	0.083
Case 2	0-2.0	0.001	0.3	8.4	4.1	3.3	0.15	0.15

855 Note: θ_r is the residual water content (L^3L^{-3}); θ_s is the saturated water content (L^3L^{-3}); K_s is the
856 saturated hydraulic conductivity (LT^{-1}); α (L^{-1}) and n (-) are parameters depending on the pore size
857 distribution; θ_f is the field capacity (L^3L^{-3}) and μ is the specific yield (-).

858

859

860 Table 2. The statistical index values of the coupled model of case 1.

	ARE (%)	*RMSE*	*IA*	R^2
Groundwater table depth (S1)	17.0	0.171 m	0.976	0.977
Soil water content at z = 1.15 m	2.2	0.008 cm^3/cm^3	0.991	0.976
Soil water content profile at t = 151 d	1.3	0.007 cm^3/cm^3	0.984	0.951
Soil water content profile at t = 212 d	4.3	0.015 cm^3/cm^3	0.976	0.914
Soil water content profile at t = 273 d	8.5	0.024 cm^3/cm^3	0.919	0.811

Scenarios				Groundwater table depth				Calculation time (s)
Number	Δt_s (d)	Δz (m)	ΔT (d)	*ARE* (%)	*RMSE* (m)	*IA*	R^2	
S1	1	0.1	5	17.0	0.171	0.976	0.977	59
S2	0.5	0.1	5	14.1	0.157	0.980	0.980	62
S3	2	0.1	5	17.7	0.157	0.979	0.958	59
S4	1	0.05	5	20.5	0.214	0.965	0.978	63
S5	1	0.2	5	24.0	0.215	0.959	0.964	60
S6	1	0.1	8	17.7	0.181	0.964	0.977	50
S7	1	0.1	10	17.3	0.124	0.988	0.977	49

861

862

863 Table 3. The statistical index values of SWMS2D and the coupled model of case 2.

Groundwater table		t = 2 h	t = 3 h	t = 4 h	t = 8 h
ARE (%)	SWMS2D	0.9%	1.5%	1.6%	1.8%
	Coupled model	11.6%	2.4%	2.9%	1.6%
RMSE (m)	SWMS2D	0.010	0.014	0.016	0.022
	Coupled model	0.088	0.025	0.029	0.021
IA	SWMS2D	0.985	0.996	0.995	0.991
	Coupled model	0.562	0.986	0.981	0.990
R^2	SWMS2D	-	0.997	0.996	0.993
	Coupled model	-	0.999	0.999	0.996

Soil water content profile		x=0.2 m	x=0.6 m	x=0.8 m	x=1.4 m	x=2 m
ARE (%)	SWMS2D	5.6%	11.4%	21.0%	17.6%	6.7%
	Coupled model	12.3%	80.5%	52.1%	27.6%	4.1%
RMSE (cm^3/cm^3)	SWMS2D	0.018	0.031	0.044	0.022	0.017
	Coupled model	0.040	0.173	0.109	0.039	0.010
IA	SWMS2D	0.863	0.828	0.919	0.990	0.962
	Coupled model	0.741	0.279	0.707	0.968	0.983
R^2	SWMS2D	0.634	0.590	0.775	0.977	0.999
	Coupled model	0.766	0.666	0.758	0.944	0.959

864

865

866 Table 4. The unsaturated hydraulic parameters of the real-world application.

Soil type	Location	θ_r (-)	θ_s (-)	K_s (m/d)	θ_f (-)
Loamy sand	Village, bared soil	0.065	0.41	1.061	0.21
Loam	Farm land	0.078	0.43	0.2496	0.24

867

868

869 Table 5. The statistical index values of the real-world application.

Water table depth	Regional average	Well 2	Well 3	Well 7	Well 8	Well 9
ARE (%)	9.9	19.4	13.9	19.7	13.5	27.9
RMSE (m)	0.203	0.253	0.233	0.383	0.241	0.366
IA	0.869	0.803	0.831	0.745	0.819	0.623
R^2	0.710	0.598	0.562	0.646	0.625	0.649

Soil water content	*t*=40 d		*t*=85 d		*t*=125 d		*t*=166 d	
	Farm land	Bared soil	Farm land	Bared soil	Farm land	Bared soil	Farm land	Bared soil
ARE (%)	15.3	10.8	15.4	19.8	15.3	16.2	24.9	14.8
RMSE (cm^3/cm^3)	0.052	0.038	0.045	0.052	0.044	0.047	0.066	0.038
IA	0.774	0.904	0.775	0.868	0.650	0.823	0.621	0.905
R^2	0.626	0.738	0.566	0.708	0.540	0.620	0.689	0.813

870

871

872 Table 6. The recharge sources and results of the tracer experiment.

	Tracer	Coupled model		
	experiment	Crop growing season	No-crop growing season	Annual
P (mm/year)	133.55	100	33.55	133.55
I (mm/year)	477.52	244.27	233.25	477.52
R (mm/year)	33.8	-56.09	92.30	36.21
R_c (-)	0.055	-	0.346	0.059

873 Note: P is the annual precipitation; I is the irrigation water; R is the annual recharge and R_c is the

874 recharge coefficient, $R_c = R/(P+I)$.

875

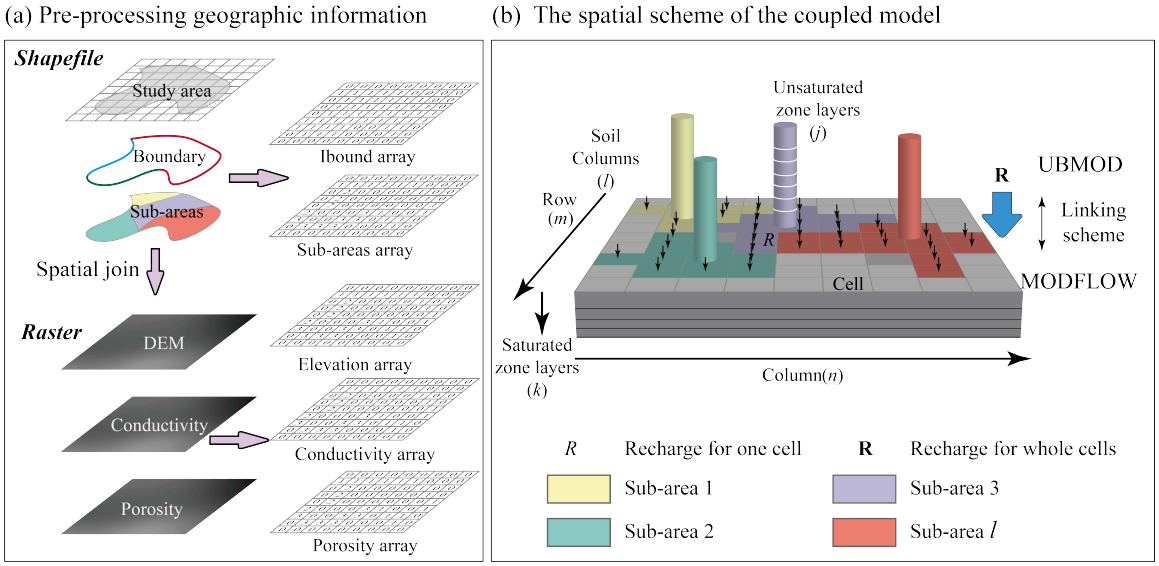

Fig. 1. (a) The procedures of geographic input information preparation. (b) The spatial scheme of the coupled model.

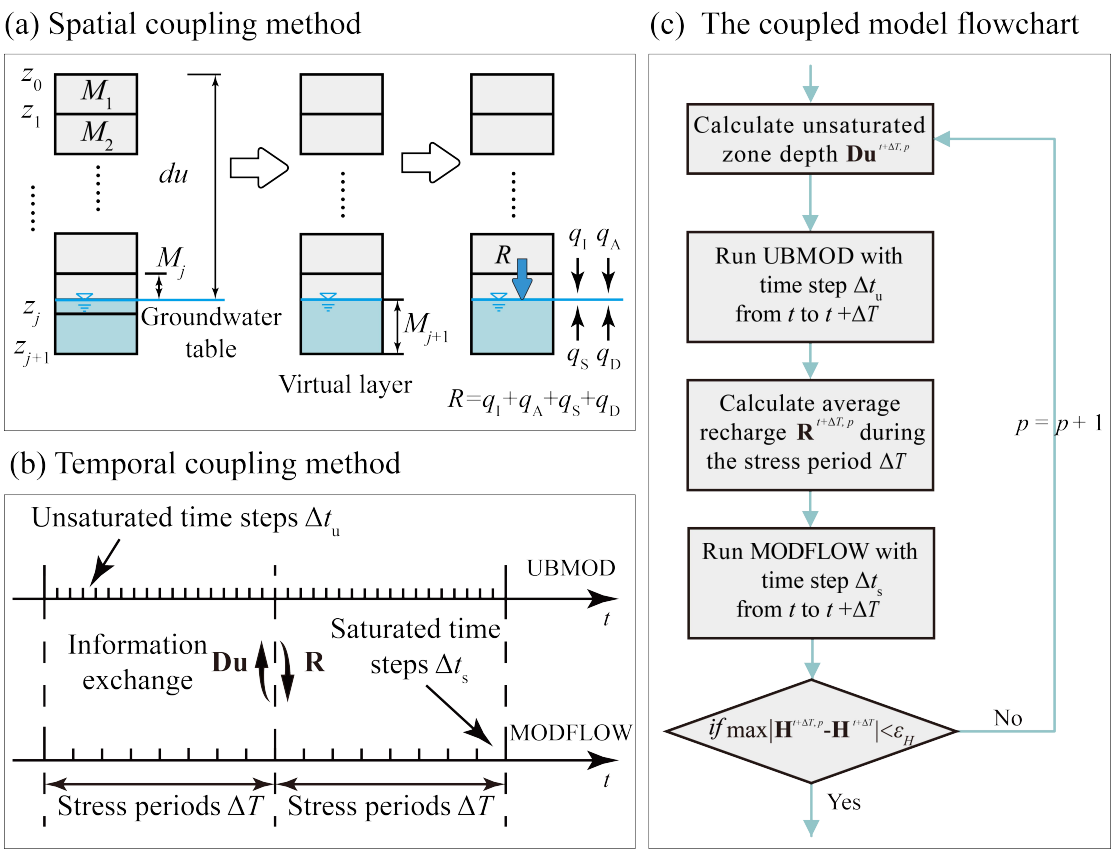

Note: z_i (i = 1, … , j) is the vertical elevation of layer i; d_u is the thickness of unsaturated zone; M_i is the thickness of layer i; R is the groundwater recharge for one cell; q_I, q_A, q_S and q_D are the fluxes across the water table caused by allocation of the infiltration water, the advective movement, source/sink terms and the water diffusion per unit area, respectively; **Du** is the thickness of unsaturated zone (l dimension); **R** is the vertical net recharge for region scale (m×n dimension); t is the time; p is the iteration level; **H** is the saturated hydraulic head (m×n dimension); ε_H is a user-specified tolerance.

Fig. 2. (a) The spatial coupling scheme for one saturated cell and one unsaturated soil column. (b) The temporal coupling scheme, and the relationship between the stress period (ΔT) and the time steps for UBMOD (Δt_u) and MODFLOW (Δt_s). (c) The specific implementation of the iterative coupling scheme from t to t+ΔT.

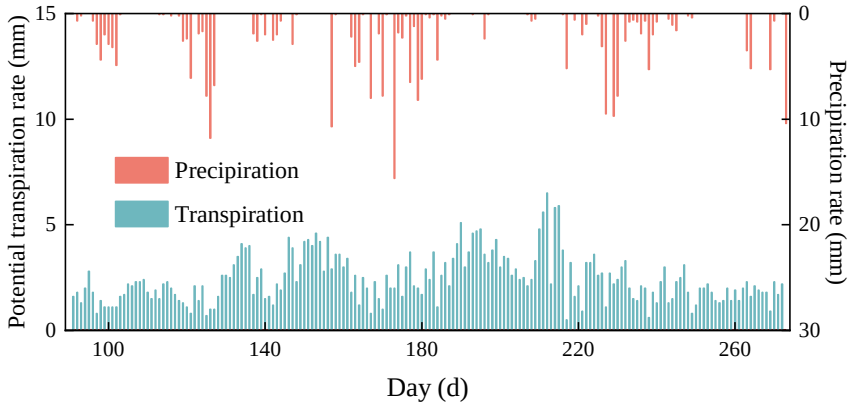

894

895 Fig. 3. The values of actual precipitation and potential transpiration rates of case 1.

896

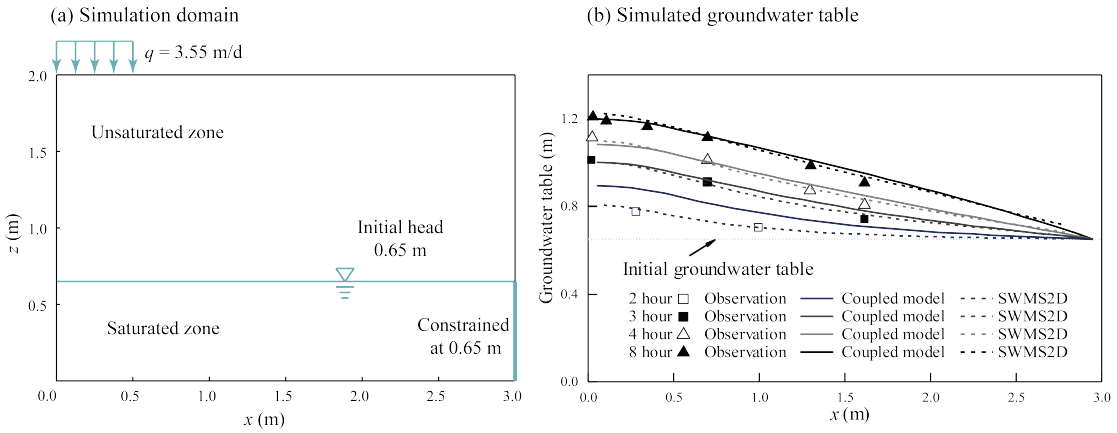

Fig. 4. (a) The sketch of the 2D recharge experiment of case 2. (b) The comparison of water table between simulated results by the coupled model, SWMS2D and observation data of case 2.

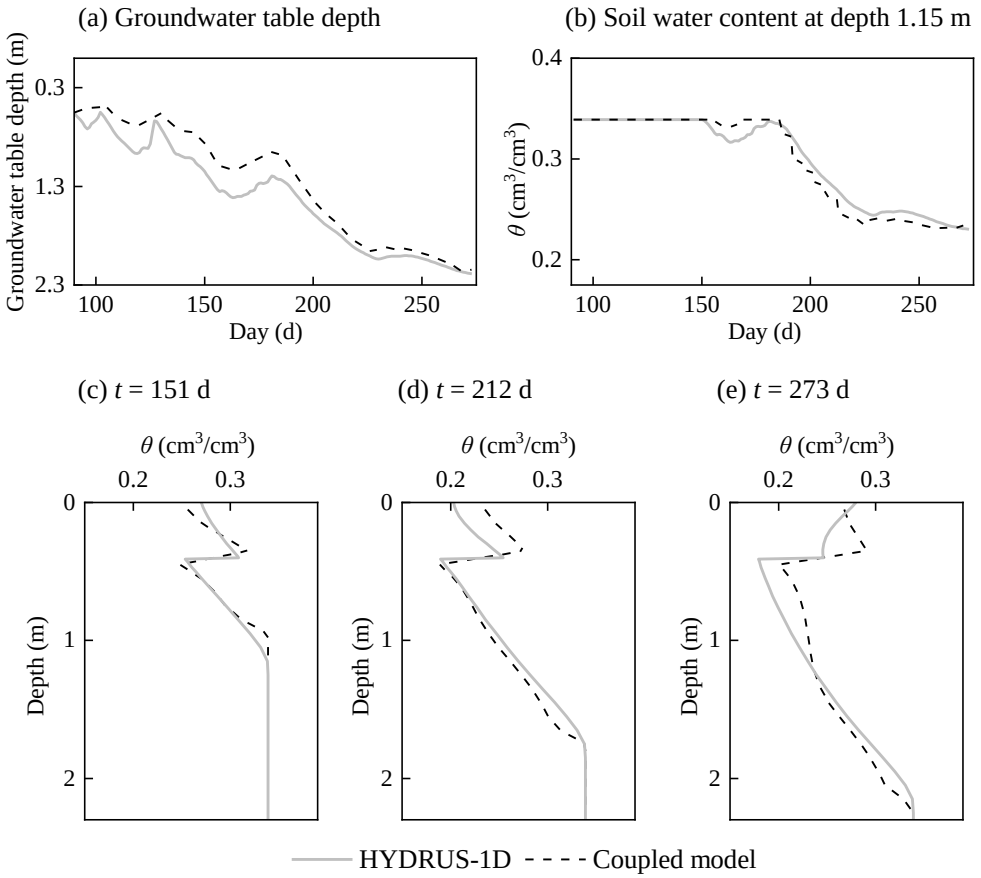

901

902 Fig. 5. The comparison of the results calculated by HYDRUS-1D and the coupled

903 model of case 1.

904

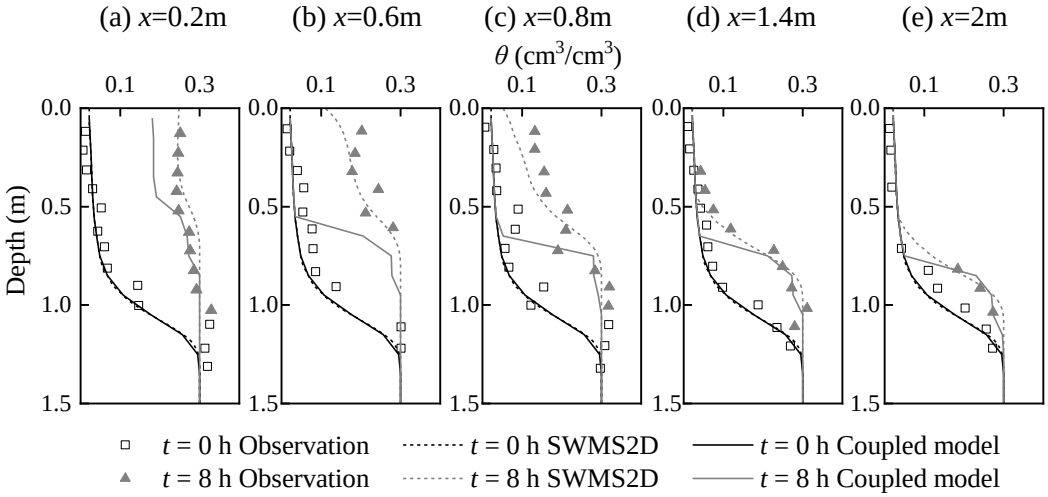

905

906 Fig. 6. Comparison of soil water content profiles between the simulations from the

907 coupled model, SWMS2D and the observations at different locations: (a) x = 0.2 m; (b)

908 x = 0.6 m; (c) x = 0.8 m; (d) x = 1.4 m; (e) x = 2 m.

909

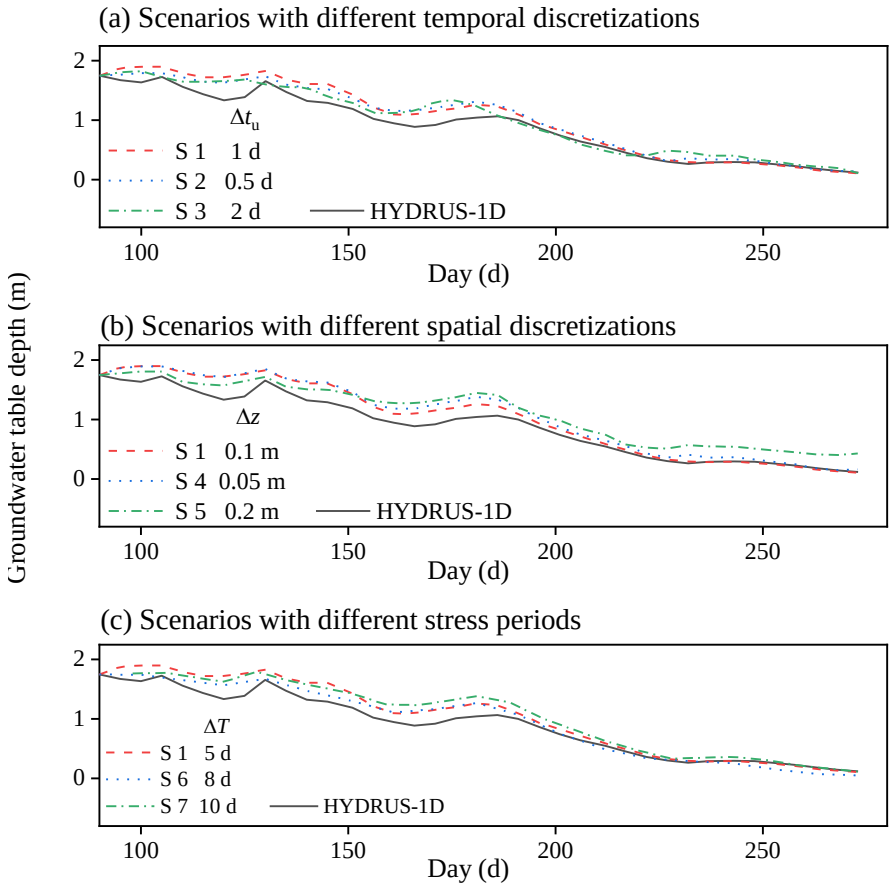

910

911 Fig. 7. The influence of (a) temporal and (b) spatial discretization and (c) stress period

912 on simulation results.

913

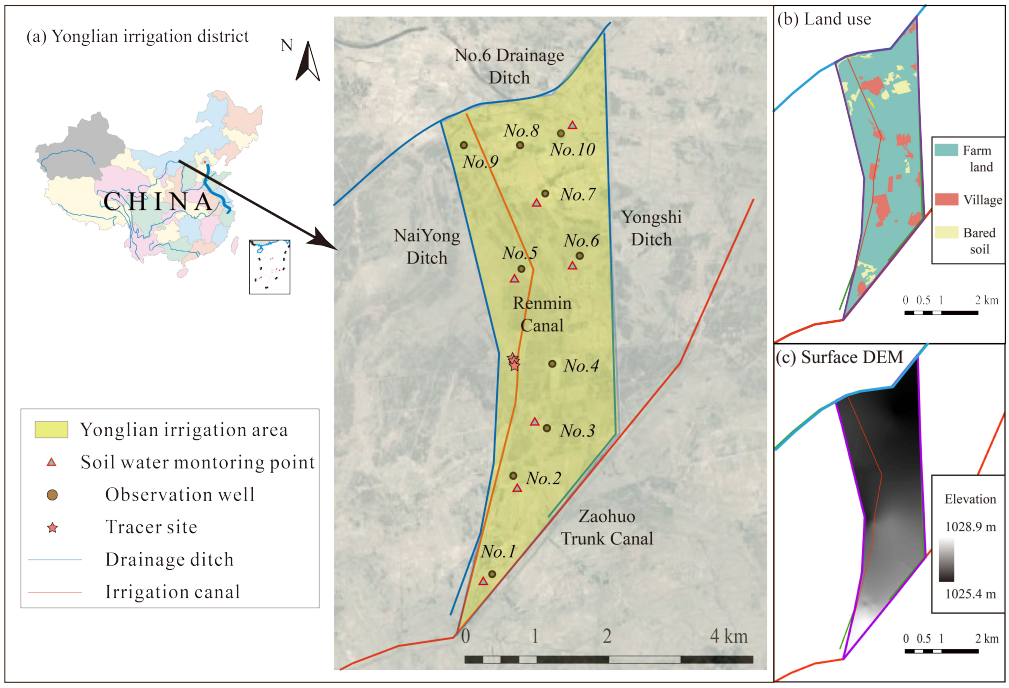

914

915 Fig. 8. (a) The geographic location of Yonglian irrigation area. (b) The land use map.

916 (c) The surface DEM.

917

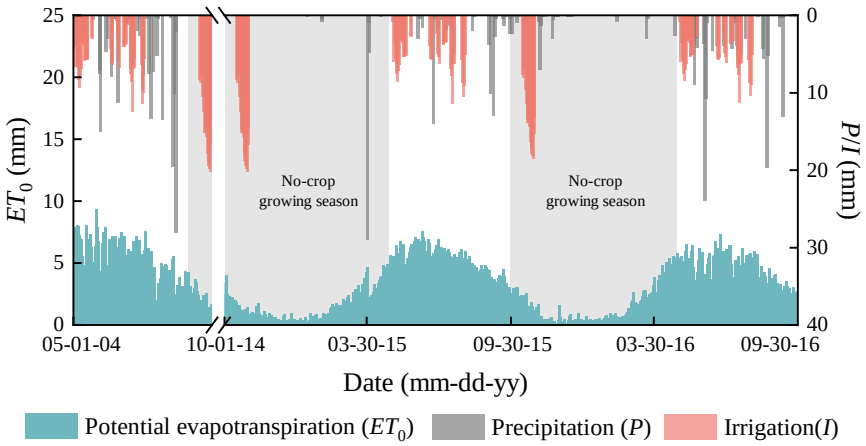

Fig. 9. Daily climate data in the Yonglian irrigation area.

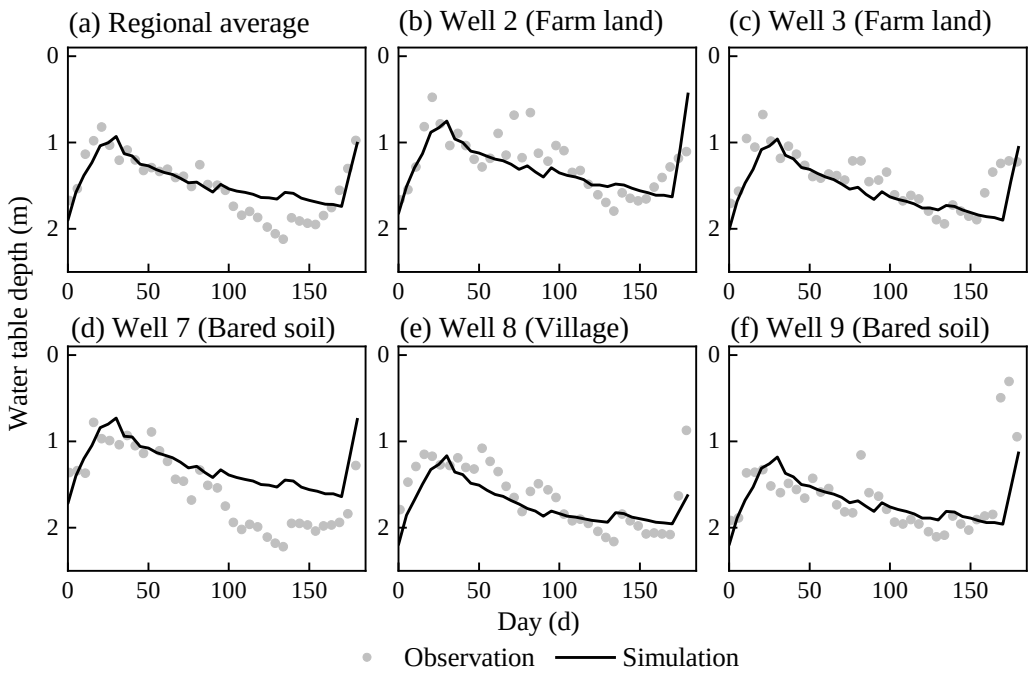

921

922 Fig. 10. Comparison between simulated and observed water table depth of the real-

923 world application.

924

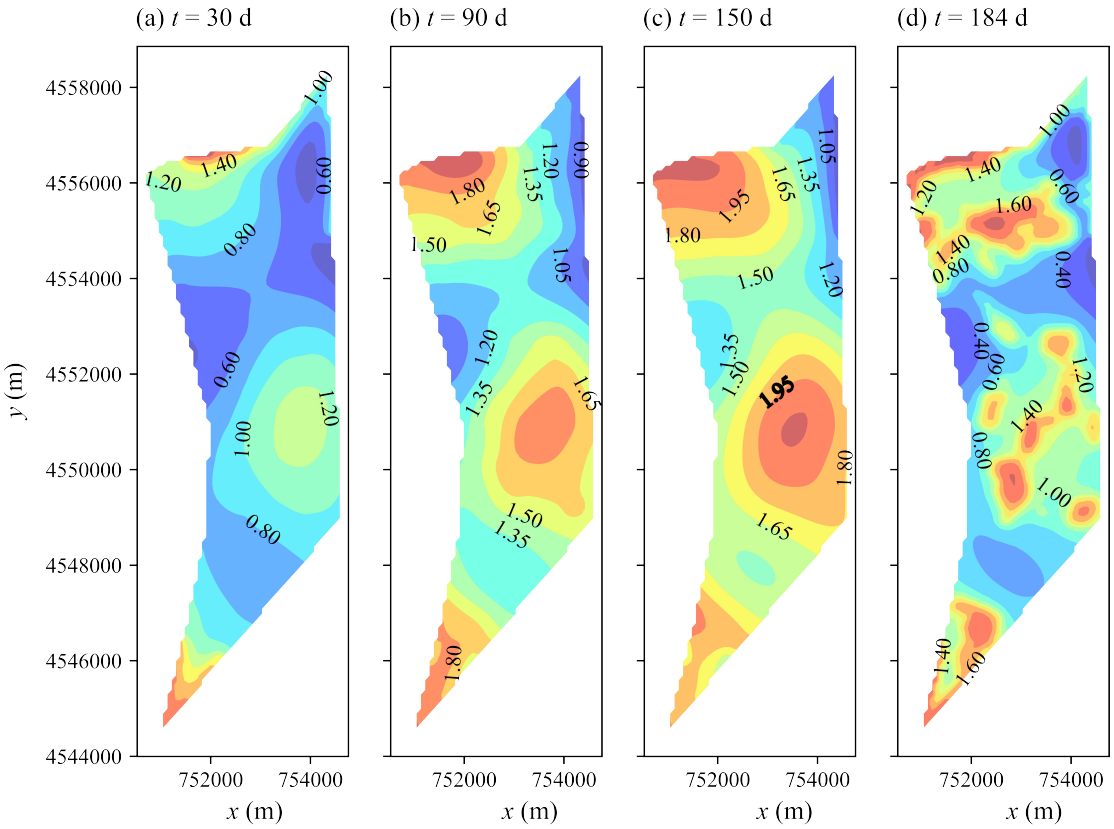

925

926 Fig. 11. Spatial simulated water table depth at different output times of the real-world

927 application.

928

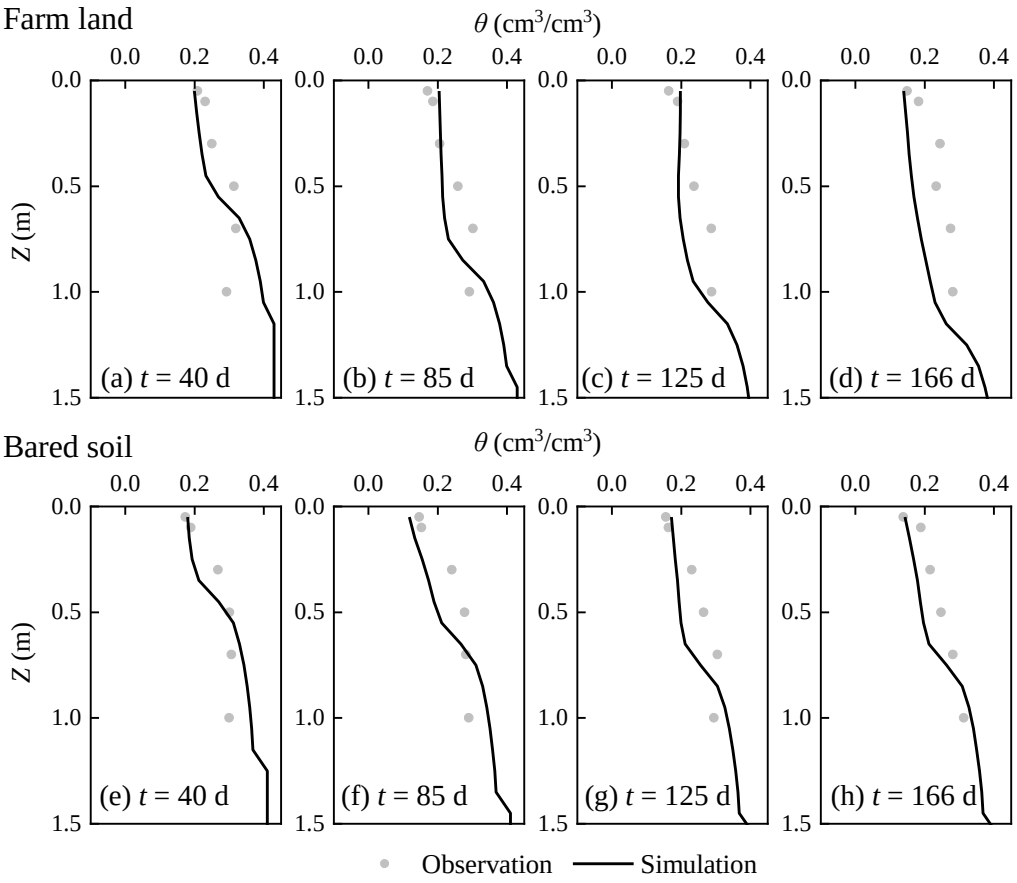

929

930 Fig. 12. Comparison between simulated and observed regional average soil water

931 content profiles of the real-world application.

932

933

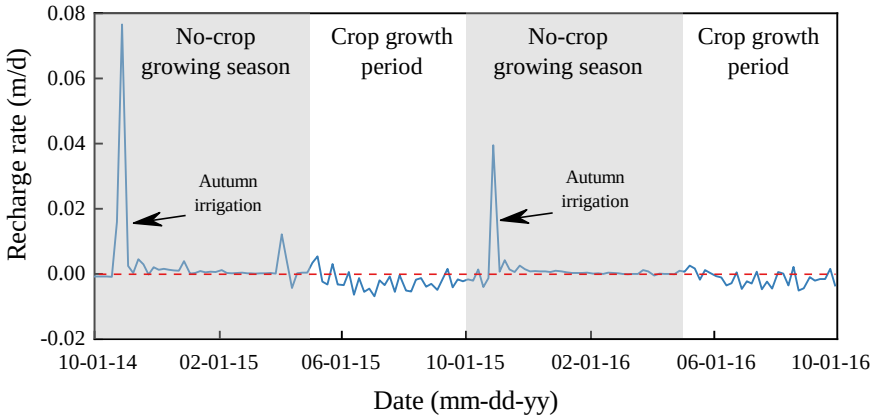

934

935 Fig. 13. The recharge rate in the farm land calculated by the coupled model

936